Current Research in Structural Biology 7 (2024) 100128

Contents lists available at ScienceDirect

Current Research in Structural Biology

journal homepage: www.journals.elsevier.com/current-research-in-structural-biology

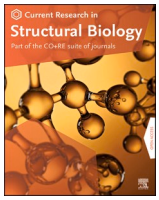

Research Article

Inhibition of *Plasmodium falciparum* plasmepsins by drugs targeting HIV-1 protease: A way forward for antimalarial drug discovery

Vandana Mishra [a,1], Anuradha Deshmukh [a,1], Ishan Rathore [a,b], Satadru Chakraborty [a], Swati Patankar [a], Alla Gustchina [b], Alexander Wlodawer [b], Rickey Y. Yada [c], Prasenjit Bhaumik [a,*]

[a] Department of Biosciences and Bioengineering, Indian Institute of Technology Bombay, Powai, Mumbai, 400076, India
[b] Protein Structure Section, Center for Structural Biology, National Cancer Institute, Frederick, MD, 21702, USA
[c] Faculty of Land and Food Systems, University of British Columbia, 248-2357 Main Mall, Vancouver, BC V6T 1Z4, Vancouver, Canada

ARTICLE INFO

Handling editor: G Oliva

Keywords:
Plasmepsins
Protease
Parasite
Malaria
Hemoglobin
Drug design
Ritonavir
Lopinavir
Inhibitors
crystal structures
Drug repurposing

ABSTRACT

Plasmodium species are causative agents of malaria, a disease that is a serious global health concern. FDA-approved HIV-1 protease inhibitors (HIV-1 PIs) have been reported to be effective in reducing the infection by *Plasmodium* parasites in the population co-infected with both HIV-1 and malaria. However, the mechanism of HIV-1 PIs in mitigating *Plasmodium* pathogenesis during malaria/HIV-1 co-infection is not fully understood. In this study we demonstrate that HIV-1 drugs ritonavir (RTV) and lopinavir (LPV) exhibit the highest inhibition activity against plasmepsin II (PMII) and plasmepsin X (PMX) of *P. falciparum.* Crystal structures of the complexes of PMII with both drugs have been determined. The inhibitors interact with PMII *via* multiple hydrogen bonding and hydrophobic interactions. The P4 moiety of RTV forms additional interactions compared to LPV and exhibits conformational flexibility in a large S4 pocket of PMII. Our study is also the first to report inhibition of *P. falciparum* PMX by RTV and the mode of binding of the drug to the PMX active site. Analysis of the crystal structures implies that PMs can accommodate bulkier groups of these inhibitors in their S4 binding pockets. Structurally similar active sites of different vacuolar and non-vacuolar PMs suggest the potential of HIV-1 PIs in targeting these enzymes with differential affinities. Our structural investigations and biochemical data emphasize PMs as crucial targets for repurposing HIV-1 PIs as antimalarial drugs.

1. Introduction

Malaria has emerged as one of the most severe infectious diseases globally and remains one of the primary causes of illness and mortality. Half of the world's population lives in malaria-endemic areas, primarily tropical and subtropical regions. In 2021, around 247 million disease incidence and 619,000 deaths were reported. Malaria affects the poorest regions of the globe, where it poses enormous health and economic challenges. Therefore, it is a priority tropical disease of the World Health Organization (World Health Organization, 2022). Among five different species of *Plasmodium* responsible for human malaria, an obligate intracellular parasite *P. falciparum* is the most virulent, resulting in the largest number of malaria-related deaths (White et al., 2014). The geographical overlap of malaria and HIV-1 infection in several parts of the world exacerbates the ferocity of the disease.

The present treatment of malaria relies on a combination of multiple drugs, such as artemisinin combination therapy, but continuous emergence of drug-resistant parasite strains against chloroquine and even against artemisinin poses a serious concern worldwide (Dondorp et al., 2009). Such challenges emphasize the urgent need to discover and develop cost-effective and potent therapeutics for economically weaker and developing countries. Therefore, drug repurposing, which includes the evaluation of approved drugs to identify their new therapeutic uses (Pushpakom et al., 2019; Rosenthal, 2003), appears as a promising approach to reduce cost and timeline for de novo drug discovery. Structural investigations of the repurposed drugs with new targets may offer chemical strategies for lead optimization, thus filling the gap between the starting hit selection and their clinical trials (Pushpakom et al., 2019).

Previous studies have reported the ability of FDA-approved HIV-1 protease inhibitors (HIV-1 PIs) to reduce the infection by *Plasmodium* parasites in the population co-infected with HIV-1 and malaria (Achan

* Corresponding author.
E-mail address: pbhaumik@iitb.ac.in (P. Bhaumik).
[1] These authors contributed equally.

https://doi.org/10.1016/j.crstbi.2024.100128
Received 22 November 2023; Received in revised form 9 January 2024; Accepted 11 January 2024
Available online 17 January 2024

Abbreviations

PMs	Plasmepsins
Hb	Hemoglobin
PMII	Plasmepsin II
PMX	Plasmepsin X
PI	Protease inhibitor
RTV	Ritonavir
LPV	Lopinavir
HIV	Human Immunodeficiency Virus

et al., 2012). The efficacy of HIV-1 PIs in reducing the *in vitro* growth of *P. falciparum* at clinically relevant concentrations has also been previously documented (Andrews et al., 2006; Skinner-Adams et al., 2004). These HIV-1 PIs have been found to be effective against other *Plasmodium* species, such as *P. chabaudi* in a murine model of malaria (Andrews et al., 2006), *P. yoelii* in the hepatic stages of rodents (Mahmoudi et al., 2008), and *P. berghei* parasites (Hobbs et al., 2009). Vacuolar plasmepsins (PMs) from *Plasmodium* have been postulated as putative drug targets of HIV-1 PIs in the co-infected population (Onchieku et al., 2018; Parikh et al., 2005). This speculation is relevant as the HIV-1 protease and the plasmepsins are homologous aspartic proteases, and therefore HIV-1 PIs might have an ability to also affect the function of PMs. Nonetheless, studies have shown that vacuolar and non-vacuolar PMs, pepsin-like aspartic proteases expressed by *Plasmodium* parasites in the human hosts, are attractive drug targets for antimalarial drug development (Banerjee et al., 2002; Boddey et al., 2010; Pino et al., 2017).

Vacuolar plasmepsins PMI, PMII, histo-aspartic protease (HAP), and PMIV (Coombs et al., 2001) are involved in the degradation of hemoglobin (Hb) in the acidic food vacuole to extract essential amino acids required for the survival of parasites (Banerjee et al., 2002). These proteases have already been recognized as drug targets for antimalarial drug discovery (Bhaumik et al., 2012); however, the functional redundancy of vacuolar PMs (Omara-Opyene et al., 2004) imposes a challenge in impeding the actions of multiple members of the plasmepsin family in order to provide efficient reduction in *Plasmodium* infection.

Besides vacuolar PMs, the indispensable roles of non-vacuolar PMs (PMV-PMX) during the parasite infection have shifted the focus of scientific community on the latter PMs and also targeting them as a strategy for antimalarial therapy. PMV is involved in the export of virulent proteins and establishment of infection in the host cell. Biochemical studies have shown that saquinavir, lopinavir, and ritonavir partially inhibit proteolytic activity of *P. falciparum* PMV (Boddey et al., 2010). PMIX and PMX are expressed at the schizont stage of asexual life cycle of the parasite, with PMX expressed as well in the liver and sexual stages in mosquito host. PMIX and PMX activate the cascades of proteins from exoneme, microneme, and rhoptry, such as SUB1, SUB2, RON3, reticulocyte-binding protein homologs (Rhs), erythrocyte binding-like proteins (EBL), which are involved in the parasite egress and invasion into host cells. The conditional knock-down studies have shown that PMIX and PMX are crucial for parasite survival inside the host cells (Favuzza et al., 2020; Nasamu et al., 2017; Pino et al., 2017), therefore should be considered as priority drug targets. Targeting PMIX and PMX would also allow multi-stage inhibition of parasite during erythrocytic egress, invasion, hepatic egress, and vector transmission due to expression of PMX in these stages of infection.

It has been shown that the peptidomimetic compound 49c and cyclic guanidine compounds such as WM4, WM382 and UCB7362 exhibit significant inhibition of these enzymes (Favuzza et al., 2020; Hodder et al., 2022; Lowe et al., 2022). Notably, our previous computational studies have demonstrated the ability of HIV-1 PIs to bind the non-vacuolar plasmepsins from *P. falciparum*, such as PMV (Bedi et al., 2016) and PMX (Kesari et al., 2022). Interestingly, lopinavir has also been shown to mediate its antimalarial effect by inhibiting the glucose transporter of *P. falciparum* (Kraft et al., 2015). Such additional targets exploited by the inhibitors might be beneficial in delaying the development of drug resistance and contributing towards cumulative antimalarial action. Targeting both vacuolar and non-vacuolar plasmepsins by HIV-1 PIs will be advantageous over a single drug target, as development of resistance against multiple targets is less likely. However, potent inhibitors targeting both vacuolar and non-vacuolar plasmepsins are still lacking. Furthermore, inhibition of PMIX and PMX by HIV-1 PIs has not been previously investigated.

For these reasons we undertook biochemical and structural studies to shed light on the molecular mechanism of inhibition of PMs by five FDA-approved HIV-1 PIs: ritonavir (RTV), lopinavir (LPV), saquinavir (SQV), nelfinavir (NFV), and indinavir (IDV). We have determined the crystal structures of PMII complexed with RTV and LPV. This is also the first report of biochemical studies of the activity of HIV-1 PIs against PMX. In addition, we analyzed the binding mode of the potent inhibitor RTV into the active site of PMX using molecular dynamics (MD) simulation studies. We have also compared the available crystal structures of pepsin-like aspartic proteases with bound RTV. Our study determined the inhibitory profile of FDA-approved HIV-1 PIs against PMII and PMX from *P. falciparum*. Knowledge of molecular details underlying the antimalarial activities of HIV-1 PIs with PMs could aid in paving the way towards designing a novel class of antimalarial drugs.

2. Results and discussion

2.1. Inhibition studies of PMs and antiparasitic activities of HIV-1 PIs

The inhibitory activity of HIV-1 PIs (RTV, LPV, SQV, NFV, and IDV) (Fig. 1) was assessed by measuring the rate of hydrolysis of the Hb-based fluorogenic peptide substrate by PMII and Rh2N fluorogenic peptide substrate by PMX, in the presence of different concentrations of inhibitors (Fig. 2A–D). All five PIs were found to be active against PMII with the K_i values in the low micromolar range of 0.3–2.4 μM (Fig. 2A and B). RTV exhibits the highest inhibitory activity against PMII with the K_i of 0.3 μM, whereas the activity of LPV is nearly two-fold lower (K_i 0.7 μM). The inhibition constants of SQV, NFV, and IDV are 1 μM, 1.4 μM, and 2.4 μM, respectively, thus showing three-to eight-fold lower activity than RTV. Such inhibition of vacuolar PMs in low micromolar range has also been reported previously (Andrews et al., 2006; Parikh et al., 2005).

The PMX zymogen (28–573) with a truncated prosegment was expressed successfully as a soluble protein (Fig. S1A). PMX zymogen was activated to form mature enzyme (Fig. S1B) which showed catalytic activity against the fluorogenic substrate (Fig. S1C). Formation of mature PMX was further confirmed by the inhibition of the enzyme by a potent inhibitor, 49c (Fig. S1D). Our data demonstrates a significant inhibition of PMX activity by RTV (K_i 0.5 μM) (Fig. 2C and D). However, LPV, SQV, and NFV inhibited PMX with lower efficiency, as indicated by the inhibition constants of 14 μM, 44 μM, and 60 μM, respectively.

The ability of RTV and LPV to arrest the growth of *P. falciparum* was further investigated in order to directly compare the IC_{50} values with the data from our biochemical inhibition assays. The *in vitro* growth of the malaria parasite in the infected RBCs pre-treated with different concentrations of inhibitors (0.1–10 μM) was assessed using flow cytometry. Both inhibitors were found to impede the asexual life cycle of the malaria parasite with modest IC_{50} values of 3.0 μM and 1.3 μM for RTV and LPV, respectively (Fig. 2E and F). The solvent control shows no inhibitory effect on the parasite. These inhibitory values are relatively higher than *in vitro* activities of inhibitors against PMII, which suggests that additional factors, such as bioavailability and off-target effects, may influence their potency at the cellular level. Notably, the higher antiparasitic activity of RTV and LPV also agrees with their *in vitro* inhibitory activities against PMII and PMX.

Antiretrovirals such as HIV-1 PIs have been shown to be effective against both chloroquine-sensitive and multidrug resistant cell lines of

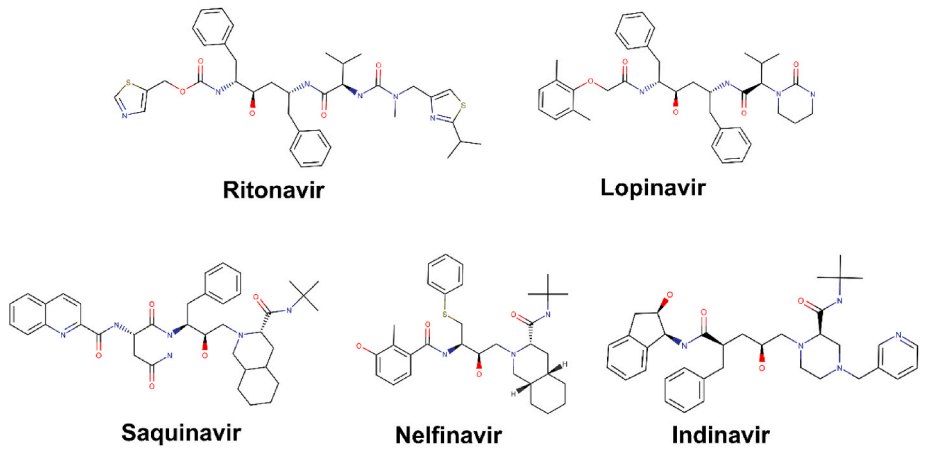

Fig. 1. Chemical structures of HIV-1 PIs used in this study.
Schematic diagrams showing the chemical structures of five FDA-approved HIV-1 PIs: Ritonavir (RTV), Lopinavir (LPV), Saquinavir (SQV), Nelfinavir (NFV), and Indinavir (IDV).

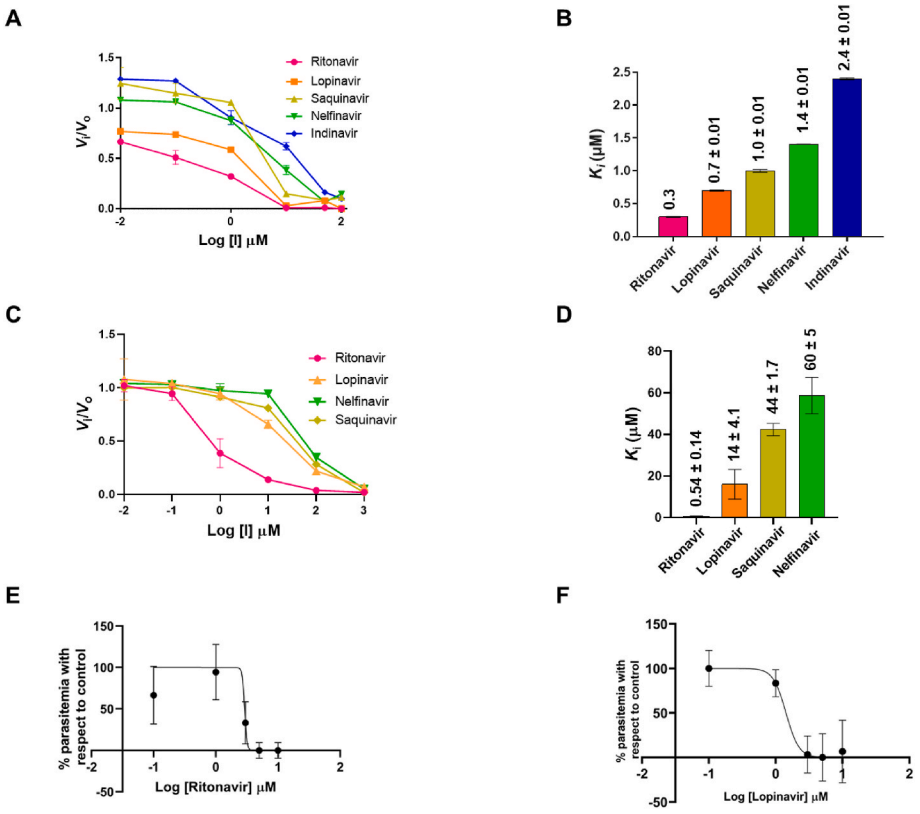

Fig. 2. Inhibition and antiparasitic activities of HIV-1 PIs. **(A)** Dose response curves of different concentrations (in μM) of HIV-1 protease inhibitors against the fractional activity of PMII. **(B)** Bar graph representing the K_i values of HIV-1 PIs against PMII. **(C)** Dose response curves of different concentrations of HIV-1 protease inhibitors against the fractional activity of PMX. (**D**) Bar diagram of K_i values of HIV-1 protease inhibitors against PMX. Dose-response curve of **(E)** RTV and **(F)** LPV, showing the log concentrations of inhibitor versus percentage parasitemia with respect to control. The experiments were performed in triplicates, and the graphs were plotted using GraphPad Prism.

parasites, including Dd2, 3D7, HB3, D6, and W2. RTV and SQV showed potent inhibition activity against a multidrug-resistant Dd2 parasite clone (Andrews et al., 2006; Parikh et al., 2005; Skinner-Adams et al., 2004). RTV and SQV have also been found to alleviate the CD36 surface concentrations on C32 cells, thus decreasing the cytoadherence of parasitized erythrocytes. Additionally, RTV has been used to enhance the circulating concentrations of other protease inhibitors in antiretroviral therapy (Gong et al., 2019), suggesting its advantage to boost the pharmacokinetics of antimalarial inhibitors. Interestingly, RTV, SQV, IDV, and NFV have been shown to aid the antimalarial activity of artemisinin and its derivatives *in vitro,* both against drug sensitive and drug resistant *P. falciparum* strains, possibly due to protease inhibition in different metabolic steps of hemoglobin digestion (He et al., 2010; Mishra et al., 2010). SQV, LPV, and tipranavir preferentially inhibited the growth of mature asexual-stage parasites 24 h post invasion. It is quite evident from our data, as well as from previous studies, that HIV-1 PIs are effective in controlling *Plasmodium* infection and should be considered for further development/repurposing as antimalarials.

2.2. Crystal structures of PMII bound to ritonavir and lopinavir

We evaluated the molecular basis of the inhibition mechanism of two relatively potent HIV-1 PIs, RTV and LPV, using protein crystallographic studies. Crystal structures of PMII complexed with RTV and LPV were determined at 1.9 Å and 3.2 Å resolution, respectively. These are the first structures of plasmepsins complexed with HIV-1 PIs. The Matthews' coefficient (Matthews, 1968) values suggested the presence of two protomers (designated A and B) in the asymmetric unit of the PMII-RTV complex, and one protomer in the PMII-LPV complex. The unambiguous F_o-F_c electron density omit maps in the active sites of the complexes indicate the presence and orientation of the inhibitors (Fig. 3A–E). The structures were refined satisfactorily as indicated by appropriate *R*-factors, acceptable stereochemical properties, and residues in the suitable Ramachandran region for their corresponding resolution range. The quality of the final $2F_o-F_c$ electron density maps in the active site is also acceptable, unambiguously defining the conformation of inhibitors, despite the comparatively low resolution of the structure of the LPV complex. Both inhibitors bind in extended conformation in the active site of PMII, with their central hydroxyl group located between the two catalytic aspartates; the flap is closed and interacts with the inhibitors (Fig. S2). CHAPS (3-[(3-cholamidopropyl) dimethylammonio]-1-propanesulfonate) is an amphipathic detergent which was added to the purification buffer during concentration and storage of protein at 4 °C. We speculate that the aggregation of protein is significantly reduced in the presence of a buffer containing CHAPS, thus indicating its role in solubilizing the protein and minimizing aggregation. Interestingly, CHAPS is bound to both protomers in the PMII-RTV complex, enclosing the active site and masking the hydrophobic surface of the protein (Fig. S3). LPV-bound PMII structure also shows the presence of

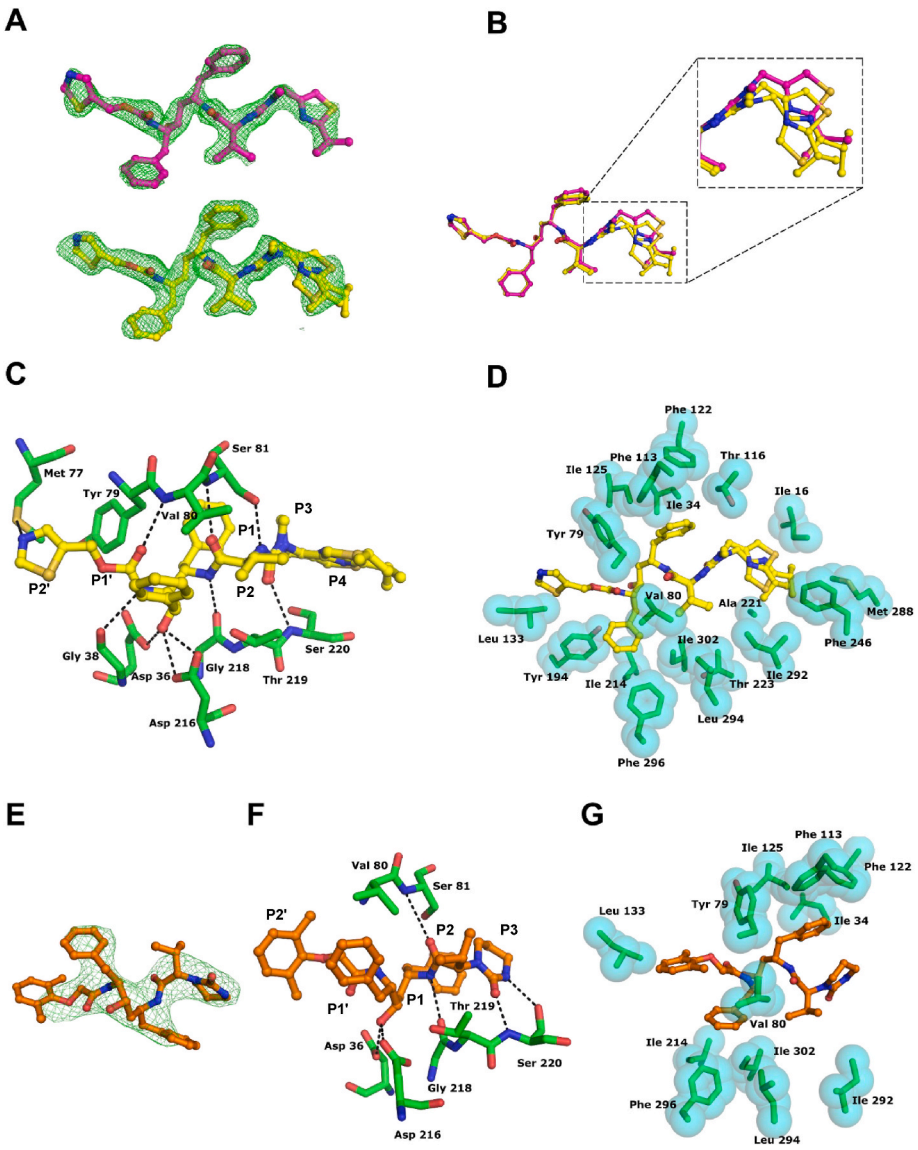

Fig. 3. Mode of binding of ritonavir (RTV) and lopinavir (LPV) to PMII. (A) Omit F_o-F_c map (contoured at 3σ level) of RTV-bound in the active site of PMII. The F_o-F_c map of two molecules of RTV from the subunits 'A' and 'B', represented in magenta and yellow, respectively; RTV in the 'B' subunit assumes a double conformation. **(B)** Superposition of RTV from the two subunits 'A' (magenta) and 'B' (yellow) of the PMII-RTV complex; inset depicts the zoomed-in-view of the region where the conformational variability exists. The binding pocket of PMII representing the **(C)** hydrogen bonding interactions in black dotted lines and **(D)** hydrophobic interactions between the protein and the inhibitor in the PMII-RTV complex shown as cyan spheres. **(E)** Omit F_o-F_c map (contoured at 2σ level) of LPV (orange) bound in the active site of PMII. The binding pocket representing the **(F)** hydrogen bonding interactions in black dotted lines and **(G)** hydrophobic interactions as cyan spheres between the protein and the inhibitor in the PMII-LPV complex. The amino acid residues in PMII are depicted as green sticks, and the inhibitors are shown in ball and stick. (For interpretation of the references to color in this figure legend, the reader is referred to the Web version of this article.)

two CHAPS molecules close to the active site. The structures indicate the essential role of CHAPS in providing stability to the protein at different stages of protein preparation. Analysis of the crystal structures of the complexes of RTV and LPV bound to PMII elucidates the molecular basis of inhibitory potency of these compounds.

2.3. Interactions of ritonavir and lopinavir with PMII

RTV comprises different functional constituents at the P1, P2, P3, P4, P1′, and P2′ positions, which are anchored *via* various hydrogen bonds and hydrophobic interactions in the active site of PMII (Fig. 3C and D). The 5-thiazo ring at the P2′ position forms a hydrogen bond with the sulfur of Met77 and a hydrophobic contact with Leu133. The P1′ of RTV is hydrogen-bonded to the carbonyl oxygen of Gly38. The carbonyl of the inhibitor interacts with the main chain amide of Val80 *via* a hydrogen bond. At the P1′ position, the phenyl ring is packed in the S1′ pocket formed by residues Tyr79, Ile214, Tyr194, and Phe296. The S1 pocket contains several hydrophobic residues (Ile34, Phe113, Thr116, Phe122, and Ile125) that tightly hold the other phenyl ring at the P1 position. The P1 amide of the inhibitor makes a hydrogen bond with the carbonyl oxygen of Gly218. The central hydroxyl group of RTV forms hydrogen bonds with the hydroxyls of active site aspartates, Asp36 and Asp216. The isopropyl moiety at P2 is further stabilized by multiple hydrophobic residues (Val80, Thr223, Ile292, Leu294, and Ile302) in the S2 pocket. The P2 carbonyl and the amide of the inhibitor engage in hydrogen bond formation with the main chain amide and the side chain hydroxyl group of Ser81, respectively. At P3, RTV makes a hydrogen bond with the main chain amide of Ser220. The P4 2-isopropyl-4-thiazolyl moiety is packed in the S4 hydrophobic pocket consisting of Ile16, Ala221, Phe246, Met288, and Ile292. A superposition of the main chain atoms of protomers A and B of the PMII-RTV complex crystal structure (r.m.s.d. 0.3 Å) indicates that most of the protein-inhibitor interactions are well conserved in both structures. Notably, at the P4 position, the inhibitor exhibits conformational variability in both protomers and is observed to exist as double conformations in protomer B of the PMII-RTV complex (Fig. 3A,B, Fig. S2B).

In the PMII-LPV complex, most of the interactions between the inhibitor and PMII are analogous to those observed in the PMII-RTV structure; however, the P1′ carbonyl group is modeled in an opposite direction in the former compared to the latter. A high-resolution structure of PMII bound LPV would further ascertain the orientation of this carbonyl group. The central hydroxyl group is engaged in hydrogen bonding with the active site aspartates (Fig. 3F). Due to bulkier aromatic functional groups in the inhibitors in the active site, hydrophobic interactions are more prominent than the hydrogen bonded contacts between the protein and the inhibitor (Fig. 3F and G). Notably, RTV has an extension at P4 that is not present in LPV, thus creating more hydrophobic contacts in the S4 pocket (Fig. 4A). Crystal structures of PMII-RTV and PMII-LPV complexes provide comprehensive insights into the binding mode of the HIV-1 PIs, enhancing the understanding of the molecular basis of the inhibition of vacuolar plasmepsins by the HIV-1 PIs.

2.4. Structural analysis of RTV-bound aspartic proteases

As plasmepsin is an aspartic protease, the superposition of PMII-RTV complex with the reported crystal structures of other aspartic proteases complexed with RTV was performed to compare their active site pockets. Superposition and structural analysis was done using PyMOL. The overlay of the atomic coordinates of the PMII-RTV complex onto crystal structures of RTV bound to HIV-1 protease (PDB ID: 1HXW), endothiapepsin (PDB ID: 3PRS), secreted aspartic proteases from *Candida albicans* (PDB ID: 3Q70) and *Candida parapsilosis* (PDB ID: 3TNE), as well as porcine pepsin (PDB ID: 6XCY) reveals that a substantial fraction of the interactions between the inhibitor and the proteins is conserved. However, the P4 moiety of RTV exhibits significant conformational variability in the S4 pocket of all RTV-bound proteases (Fig. 4B). In all structures, the S4 pocket has been found to accommodate additional small molecules, such as ethylene glycol, DMSO, and CHAPS, derived either from the purification buffer, mother liquor, or cryoprotectant, highlighting the larger volume of the S4 pocket. These small molecules are found to interact with the protein and the inhibitor, affecting orientation of certain groups in RTV. Therefore, the conformational flexibility of the P4 moiety is plausibly governed by the presence of small molecules wedged into or close to the S4 pocket. These molecules might create steric hindrance based on their size, shape, and orientation, moving the P4 moiety in these structures. Notably, the P4 group of RTV in the PMII-RTV complex has shifted relative to other RTV-bound protease structures. Other deep pockets have similar, relatively well conserved residues in both vacuolar and non-vacuolar PMs, with the inhibitor side chains well packed. Therefore, larger volume of the S4 pocket in RTV-bound aspartic protease structures can be exploited to improve the potency of the HIV-1 PIs to target various members of the plasmepsin family.

2.5. Comparison of different classes of inhibitors in PMII active site

Superposition of the crystal structure of the complex of RTV with PMII presented in this study with the structures of the previously reported peptidomimetic, non-peptidomimetic, and achiral inhibitors has been performed in order to compare their binding mode (Fig. 5). The binding orientation of RTV is similar to that of pepstatin A (a highly

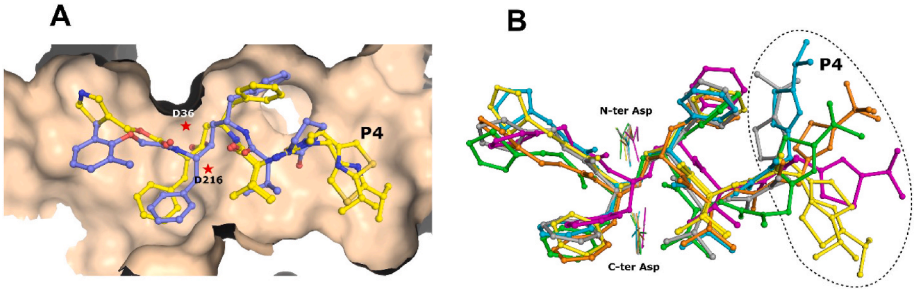

Fig. 4. A comparison of the binding modes of HIV-1 PIs in the active site of aspartic proteases. **(A)** Surface representation of the superposed structures of ritonavir (RTV, yellow) and lopinavir (LPV, blue) bound to PMII. Due to the P4 extension in RTV compared to LPV, the former creates additional hydrophobic contacts in the S4 pocket. The catalytic aspartates are marked with red stars and labeled. **(B)** Superposition of RTV-bound PMII complex (yellow) with the available crystal structures of RTV complexed with other aspartic proteases: HIV-1 protease (PDB ID:1HXW) in cyan, endothiapepsin (PDB ID: 3PRS) in orange, secreted aspartic protease (PDB ID: 3Q70) in gray, Sapp1 (PDB ID: 3TNE) in green, and porcine pepsin (PDB ID: 6XCY) in magenta; all represented as ball and stick models. The superposed structures demonstrate the conformational flexibility at the P4 position of the inhibitor (region marked in black dashed lines) in the RTV-bound aspartic protease crystal structures. The two active site aspartates are represented in the sticks and are labeled. (For interpretation of the references to color in this figure legend, the reader is referred to the Web version of this article.)

potent, but non-specific aspartic protease inhibitor with K_i of 0.006 nM (Silva et al., 1996)) (PDB ID: 1XDH) (Fig. 5A) and its analogs (PDB ID: 1XE5, 1XE6). However, most of the polar groups in pepstatin A are substituted by hydrophobic moieties in RTV. Comparison with the kynostatin inhibitor series with K_i in low nanomolar range from 1 to 6 nM (Mishra et al., 2018)(PDB IDs: 5YIA, 5YIB, 5YIC, 5YID, and 5YIE) reveals the opposite orientation of RTV and the utilization of different pockets. The P3′ moiety in KNI-10333 shows distinct conformation and shifts towards the flap outside of the active site pocket (Fig. 5B) (Mishra et al., 2018).

The binding of transition-state mimicking inhibitors RS367 (PDB ID: 1LEE) and RS370 (PDB ID: 1LF2), with K_i of 18 and 30 nM, respectively (Asojo et al., 2002), as well as EH58 (PDB ID: 1LF3), a potent non-peptidomimetic inhibitor with K_i 100 nM (Asojo et al., 2003), assume the same pose as RTV in the active site pocket of PMII (Fig. 5C and D). Achiral inhibitors (PDB IDs: 2BJU, 2IGX with IC_{50} of 34 and 54 nM, respectively) (Boss et al., 2006; Prade et al., 2005), and a non-peptidomimetic inhibitor DR718A (PDB ID: 4Z22 with IC_{50} of 340 nM) (Recacha et al., 2015) bind unusually deep into the flap pocket (Fig. 5E). RTV binds in a much more extended conformation compared to the hydroxyethylamine-based inhibitors (PDB IDs: 4CKU with IC_{50} of 150 nM (Jaudzems et al., 2014), 4Y6M, 4YA8) The latter inhibitors are shorter than RTV and cannot extend to reach the S4 pocket. We also observed different orientations of the P3 groups. The bulkier groups at P1, P4, P1′, and P2′ in RTV imply that the respective pockets in PMII can fit larger moieties (Fig. 5F).

Structural analysis demonstrates that the large volume of deep pockets in PMII and inherent plasticity of residues lining its active site can accommodate diverse classes of inhibitors that differ in their chemical structures, size, and shape. The active site favors both hydrogen bonding and hydrophobic interactions due to the distribution of polar and non-polar groups. Such plasticity might be important in combination therapy where synergistic actions of two or more classes of drugs are needed to mitigate the effects of *Plasmodium* pathogenesis.

2.6. Binding mode of ritonavir in the active site of plasmepsin X

In addition to inhibiting vacuolar PMII, FDA-approved HIV-1 PIs can also inhibit non-vacuolar PMV. The molecular basis of the binding of SQV to *P. falciparum* PMV has been studied previously (Bedi et al., 2016). In this study we report mechanistic details of inhibition of PMX by RTV using an all-atom MD simulation approach for 100 ns (Fig. 6, Fig. S4). The PMX-RTV complex remains stable throughout the simulation process, as observed in the RMSD plot (Fig. S4A). The flap (Ile303-Thr322) and the adjacent helix (Ile354-Ile358) of PMX attain a conformation that is different from the initial position observed in the crystal structure of a complex with inhibitor TWU (PDB ID: 8DSR). This observation indicates the binding process of the peptidomimetic inhibitor RTV is different than the cyclic acyl guanidine scaffold-based inhibitor TWU (Lowe et al., 2022), which leads to different flap conformation (Fig. S4C). Analysis of the PMX-RTV complex shows that the central hydroxyl group of the inhibitor interacts with the N-terminal

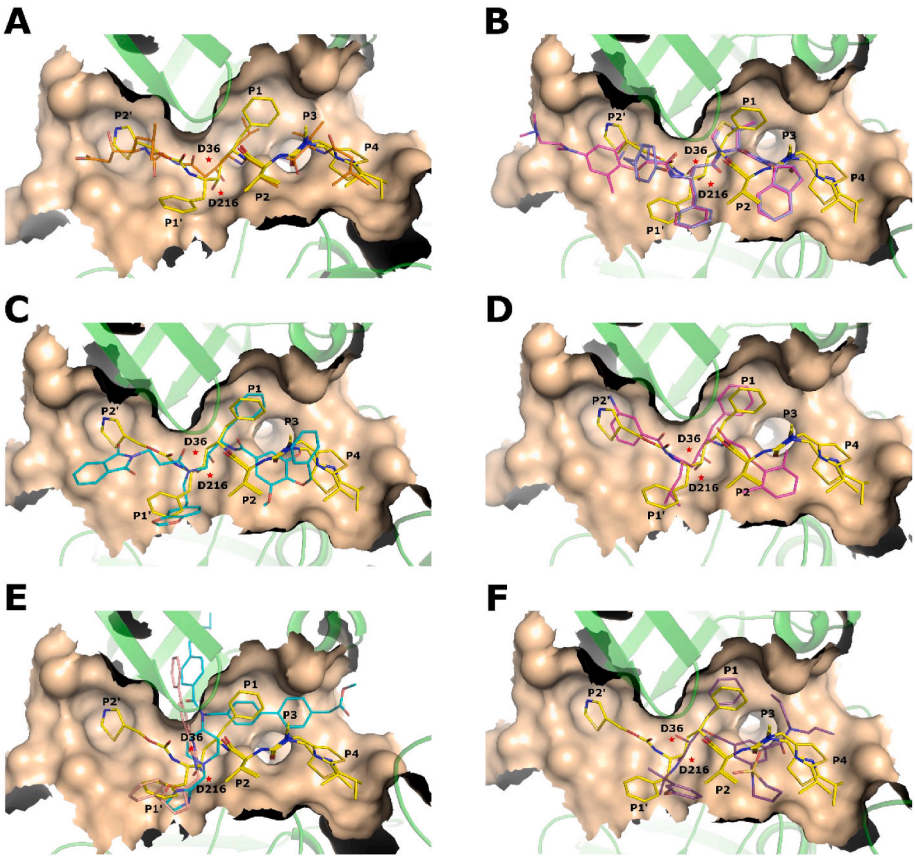

Fig. 5. Binding modes of different classes of inhibitors in the PMII active site. **(A)** Surface representation of the superposed structures of ritonavir (RTV, yellow) with pepstatin A in orange (PDB ID: 1XDH), **(B)** KNI-10743 in magenta (PDB ID: 5YIB) and KNI-10333 in blue (PDB ID: 5YIC), **(C)** non-peptidomimetic EH58 inhibitor in cyan (PDB ID: 1LF3), **(D)** peptidomimetic RS367 inhibitor in magenta (PDB ID: 1LEE), **(E)** achiral inhibitor in cyan (PDB ID: 2BJU) and non-peptidomimetic inhibitor DR718A in salmon (PDB: 4Z22), **(F)** hydroxyethylamine-based inhibitor in purple (PDB ID: 4CKU). The catalytic aspartates are marked with red stars and labeled. All inhibitors are represented as sticks. The active site region is shown as surface and other parts of protein is represented as green cartoon. The superposed structures of inhibitors-bound PMII structures demonstrate the similar binding mode of HIV-1 PIs and other peptidomimetic inhibitors while utilizing comparable or additional pockets. Certain groups in the achiral and non-peptidic inhibitors are moved in the flap region. The two active site aspartates are represented as red asterisks and labeled. (For interpretation of the references to color in this figure legend, the reader is referred to the Web version of this article.)

Asp266 throughout the simulation process by forming a hydrogen bond with either OD2 or OD1 (Fig. 6A–C); a similar interaction is observed in the SQV-endothiapepsin complex (PDB ID: 3PWW) (Behnen et al., 2012). Notably, two other important water molecules are present between Ser269 and Trp273 and form a hydrogen bonding network in the active site (Fig. 6A) in the absence of the usual Tyr, which is substituted by Phe311 in PMX. Two water molecules at the identical positions are also observed in the crystal structures of apo PMX (PDB ID:7TBB) from *P. falciparum* and WM382 bound PMX (PDB ID: 7TBD) from *P. vivax* (Hodder et al., 2022).

The RTV inhibitor interacts through hydrogen bonding and hydrophobic interactions with the same subsites of the active site pocket of PMX as in PMII (Fig. 6D). The 5-thiazo ring is inserted into the S2′ subsite of PMX and forms S-π interaction with Met371 and alkyl-π interaction with Ile309 (Fig. 6B). Besides that, the N5 atom of the 5-thiazo ring forms hydrogen bonding interaction with the backbone of Thr270 and Met371 through a water molecule (Fig. 6A). The backbone O24 atom is present next to the 5-thiazo ring, forming a stable hydrogen bond with a water molecule (Fig. 6A). The phenyl group at P1′ of the RTV is surrounded mainly by hydrophobic residues e.g., Ile455, Tyr431, Ile528, and Leu539 (Fig. 6B–D). Residues lining of the S1′ pocket are primarily hydrophobic and usually interact with a phenyl group of the substrate (Kesari et al., 2022). Residues Phe311 and Phe360 form π-π stacking interaction with the phenyl group at the P1 position (Fig. 6B). The carbonyl group next to the phenyl group forms a stable hydrogen bond with the side chain of Ser313 that is located in the flap (Fig. 6A; Fig. S4B). The S2 pocket harbors the isopropyl group of RTV. The P3 moiety forms a hydrogen bond with a water molecule trapped between the backbones of Gln247 and Gly459 (Fig. 6A). The P4 2-isopropyl-4-thiazolyl moiety makes S-π and alkyl-π interactions with Met526 and Ile354, respectively (Fig. 6B). The orientation of the P4 moiety is different compared to its equivalent in the complexes with PMII and other aspartic proteases. While comparing the RTV binding sites of PMX with PMII, the inhibitor was found to occupy the same subsites S2′, S1′, S1, and S2 of the active site (Fig. 6D); S1′ and S1 pockets of both enzymes also exhibit preferences for the same residues of the substrates (Leu for S1′, Phe for S1) (Favuzza et al., 2020; Istvan and Goldberg, 2005).

2.7. Active site pocket analysis of vacuolar and non-vacuolar plasmepsins

Analysis of the active site pockets of all four vacuolar PMs (PMI, PMII, HAP, and PMIV) reveals that many residues that form them are conserved, and so is the pocket volume (Fig. 7). HAP has some substitutions by residues of similar size in its active site compared to other vacuolar PMs. Structural analysis of the active site pockets in PMII and PMX reveals analogous interactions with HIV-1 PIs, indicating that most of the pocket substitutions are relatively well conserved (Fig. 7). The N-terminal moieties and the central core of the inhibitor are prominently stabilized by similar amino acid substitutions in PMX, which primarily include hydrophobic interactions and a few hydrogen bonding contacts.

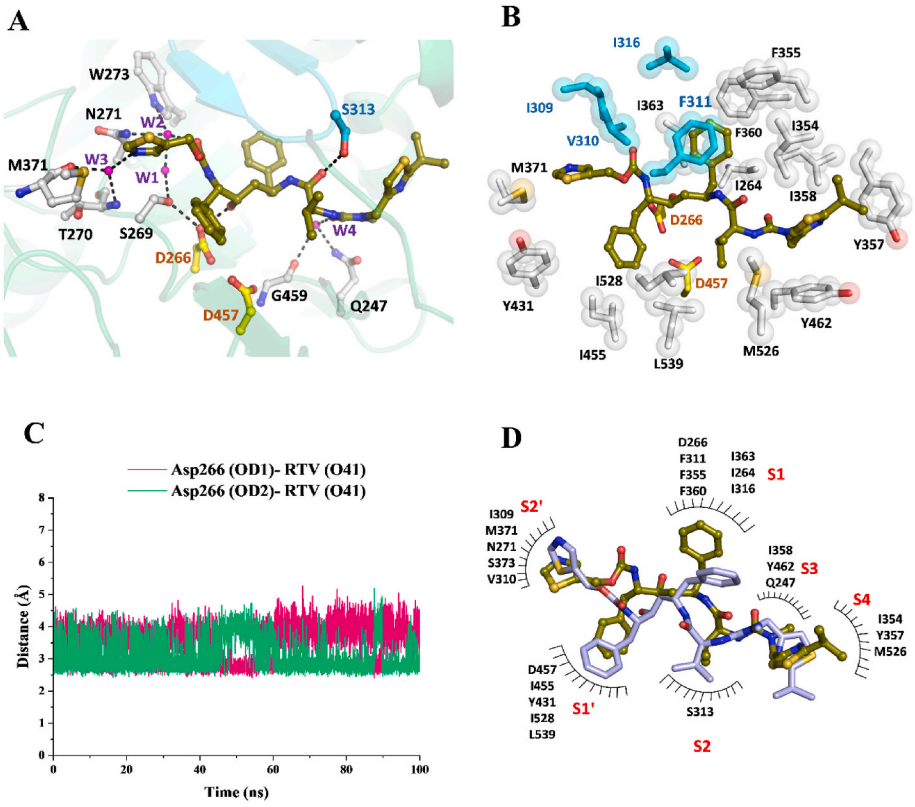

Fig. 6. Binding mode of Ritonavir (RTV) in the active site of plasmepsin X (PMX). (A) Hydrogen bonding interactions formed by RTV with PMX. The RTV molecule is represented by deep olive-colored carbon in ball and stick model. The catalytic Asp266 and Asp457 are represented in yellow-colored carbon, while other important residues are in gray-colored ball and sticks. The water molecules present in the active site are represented in magenta spheres. The hydrogen bonding interactions are marked in black dashed lines. The overall protein secondary structure is represented in green cartoon. The flap region is shown in cyan cartoon and the flap residues present in the active site are represented in cyan ball and stick model. **(B)** The residues forming hydrophobic interactions are represented in gray spheres and sticks. RTV molecule is represented in deep olive-colored ball and sticks. The catalytic Asp266 and Asp457 are represented in yellow-colored carbon. The flap active site residues are shown in cyan sphere and sticks. **(C)** The stable hydrogen bonding interactions between catalytic Asp266 OD1 and OD2 atoms with O41 atom of the RTV during MD simulation. **(D)** Comparison of the binding mode of RTV molecule to PMX with the binding mode of RTV to plasmepsin II (PMII). RTV bound to PMII crystal structure is represented by light blue color sticks and RTV interacting with PMX is represented by deep olive ball and sticks. The schematic representation of RTV binding in different subsites of PMX is shown around the ball and stick model of RTV. (For interpretation of the references to color in this figure legend, the reader is referred to the Web version of this article.)

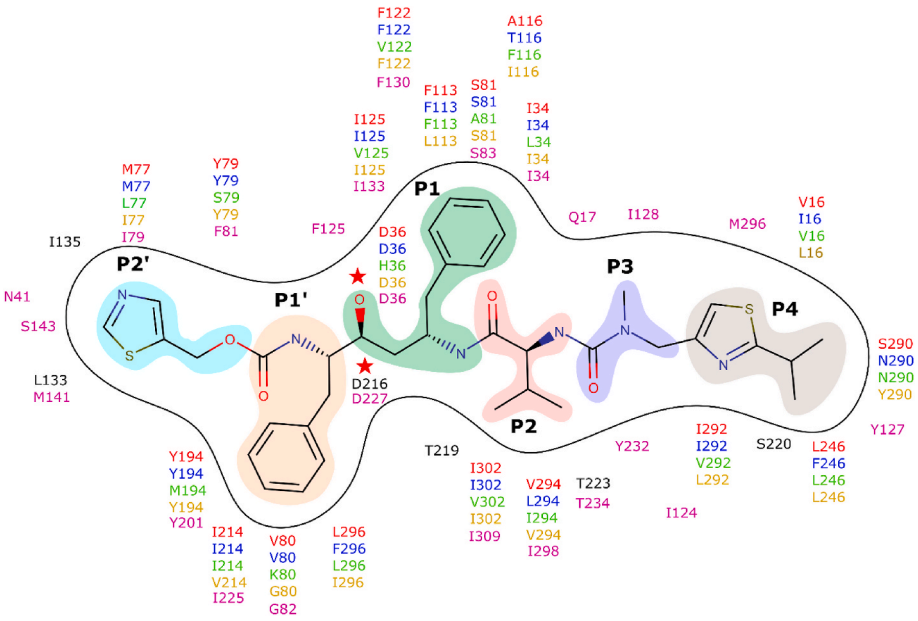

Fig. 7. Schematic showing a comparison of RTV-binding pocket of PMII with other vacuolar PMs and non-vacuolar PMX.
Different residues lining the binding pockets of vacuolar plasmepsins PMI (red), PMII (blue), HAP (green), and PMIV (yellow) are labeled. If the amino acids are conserved in all the vacuolar PMs, they are labeled as black. The residues located in the binding pocket of non-vacuolar plasmepsin X are labeled in magenta. The two active site aspartates are represented as red asterisks and labeled. Most of the residues are conserved or substituted by residues with similar properties in both vacuolar and non-vacuolar PMs. (For interpretation of the references to color in this figure legend, the reader is referred to the Web version of this article.)

Additionally, the large volume of the S4 pocket in PMX suggests that the flexible P4 group can freely explore different regions within the pocket. Such interactions are also evident in the crystal structure of the PMII-RTV complex. Thus, it is likely that RTV and LPV have a potential to target multiple vacuolar and non-vacuolar PMs. This would be a crucial feature of these inhibitors, considering the overlapping functions and pivotal roles of PMs. The structural findings outlined in this study illustrate the efficacy of HIV-1 PIs in inhibiting the functions of PMs. Moreover, these inhibitors hold potential for further structure guided refinement to augment their effectiveness as antimalarial agents.

3. Conclusion

Development of resistance against the currently used antimalarial drugs is of major concern. Repurposing HIV-1 PIs emerges as a promising and expeditious approach to address this issue. Pepsin-like aspartic proteases are known to be attractive drug targets for the treatment of both HIV-1 caused AIDS, as well as for malaria. Structure-based studies are instrumental in unraveling the mechanism of inhibition of aspartic proteases in these disease-causing agents.

We have studied the inhibition of vacuolar and non-vacuolar plasmepsins by five HIV-1 PIs which all are FDA-approved antiretroviral drugs. Among the tested inhibitors, RTV shows the highest inhibition constant for both PMII and PMX. Crystal structures of a vacuolar plasmepsin, PMII, complexed with RTV and LPV, as well as molecular dynamics studies of the interactions of RTV with PMX provide structural insights to guide the process of further antimalarial drug development. In various RTV-bound aspartic protease structures, RTV displays conformational flexibility at the P4 position, implying that substitutions at this position could be well accommodated in the large S4 pocket. Therefore, introducing modifications at the P4 position of RTV could potentially enhance its binding affinities against both vacuolar and non-vacuolar plasmepsins. We have also demonstrated the binding of RTV to the active site of PMX. Crystal structures and MD simulation studies unveil the interactions at the molecular level and validate HIV-1 PIs as legitimate drug targets for both vacuolar and non-vacuolar plasmepsins. Structural analysis also sheds a light on the mechanism of differential inhibitory activity of these compounds in biochemical assays. Owing to the ability of HIV-1 PIs to target both vacuolar and non-vacuolar PMs, it should be possible to design effective broad-spectrum protease inhibitors based on structure-activity relationships. Analysis of the active site pocket of all four vacuolar PMs (PMI, PMII, HAP, and PMIV) and non-vacuolar PMX reveals that many residues are conserved, and thus is the volume of the pocket. Our biochemical and structural investigations should help in finding new leads that might assist in designing novel antimalarial candidates against a range of related pathogenic proteases implicated in infectious diseases.

4. Materials and methods

4.1. Inhibition of PMII by HIV-1 PIs

Expression and purification of recombinant, soluble thioredoxin-tagged truncated PMII (Trx-tPMII) was performed as described previously (Mishra et al., 2018), with a few modifications. The primary and secondary culture of bacteria (Rosetta-gami B(DE3) pLysS) were grown in Terrific Broth media at 28 °C overnight to achieve higher expression levels of soluble Trx-tPMII.

Five FDA-approved HIV-1 PIs used in this study (RTV, LPV, SQV, NFV, and IDV) were purchased from Sigma-Aldrich (St. Louis, MO). Except for IDV which is soluble in double distilled water, the other four inhibitors were dissolved in 100% dimethylsulfoxide (DMSO). Aliquots of stock solutions of inhibitors (10 mM) were stored at −20 °C. Inhibition assays were performed as reported earlier (Mishra et al., 2018). To measure the proteolytic activity of mature PMII, the internally quenched fluorescent synthetic peptide substrate EDANS–CO–CH_2-CH_2-CO-Ala-Leu-Glu-Arg-Met-Phe-Leu-Ser-Phe-Pro-Dap-(DABCYL)-OH (AnaSpec In c., Fremont, CA, USA), was used. The enzyme was pretreated for 5 min with the HIV-1 PIs in a concentration range of 0.1–100 μM at 25 °C in 0.1 M sodium acetate buffer pH 5.0, followed by the addition of 1 μM concentration of substrate. Hydrolysis of the substrate was monitored at each inhibitor concentration. The assays were performed in triplicates at 25 °C pH 5.0. Data were fit to sigmoidal dose-response curves with nonlinear regression to calculate IC_{50} values using GraphPad Prism

(version 8.0). IC_{50} values were converted to K_i values using the Cheng-Prusoff equation for competitive inhibitors, $K_i = IC_{50}/(1+[S]/K_m)$ (Cheng and Prusoff, 1973).

4.2. Expression and purification of PMX

P. falciparum PMX gene (28–573) with a truncated prosegment (28–234) was cloned into the pMAL-C2X vector containing an MBP tag at the N terminus and a His_6 tag at the C terminus (Fig. S1). C-terminal tag was introduced with a suitable primer during the PCR amplification of the gene. The recombinant protein was expressed in the SHuffle T7 Express lysY cell (New England Biolabs) by inducing with 1 mM IPTG at 18 °C for 14 h. The cell pellet was suspended into equilibration buffer (25 mM Tris, 200 mM NaCl, 1 mM EDTA pH 8.0) and the suspension was lysed by sonication with 40% amplitude for 15 min. The lysate was centrifuged at 16,000 g for 30 min and the supernatant containing a soluble fraction of protein was used for purification. This soluble fraction was loaded onto the MBPTrap dextrin column (Cytiva) equilibrated with buffer. The contaminants were removed by passing the 5-column volume equilibration buffer. The bound MBP-tagged PMX was eluted with 100% elution buffer (25 mM Tris, 200 mM NaCl, 1 mM EDTA, 10 mM maltose pH 8.0). The eluted protein was diluted with ion exchange equilibration buffer (25 mM Tris, pH 8.0) and loaded on the HiTrap DEAE Sepharose FF column (Cytiva). The elution of bound protein was carried out by 10%, 20% and 20–100% gradient with elution buffer (25 mM Tris, 1 M NaCl, pH 8.0). The eluted protein was subjected to maturation (Fig. S1A).

We also created a D457A active site mutant of PMX which was expressed and purified following a similar procedure.

4.3. Inhibition assays of PMX by HIV-1 PIs

The purified protein was buffer exchanged with 25 mM HEPES, pH 8.0 and incubated at 4 °C overnight for maturation. The mature enzyme was used for activity and inhibition assays. An internally quenched Rh2N synthetic peptide (Dabcyl)-HSFIQEGKEE(Edans)-NH_2 was used to check the enzyme activity (Favuzza et al., 2020) of mature PMX. The peptide cleavage with an active enzyme leads to the increase in fluorescence with time. The protein sample was mixed with assay buffer (25 mM Na acetate, 0.005% Tween-20, pH 5.5) and concentration range (0.01 μM–1000 μM) of HIV-1 protease inhibitors and 49c (0.5 nM–20 nM) (49c was the kind gift from Prof. Dominique Soldati-Favre), followed by addition with 1 μM of substrate. The fluorescence was measured at the excitation wavelength 340 nm and emission wavelength 500 nm and recorded with BMG LABTECH plate reader (VANTAstar). Data was plotted using a similar method as described for PMII.

4.4. Antiparasitic assays

For an antiparasitic assay, malaria parasite *P. falciparum* 3D7 was cultured on human O+ erythrocytes maintaining 2% hematocrit with 5% CO_2, 1% O_2, and 94% N_2 environment in RPMI (Roswell Park Memorial Institute, Gibco, Grand Island, NY, USA) medium supplemented with Albumax 5 g/l, glucose 2 g/l, sodium bicarbonate 2 g/l, hypoxanthine 55 mg/l, and gentamycin 40 μg/ml (Cranmer et al., 1997; Zolg et al., 1982). Synchronization of the parasite was done with 5% D-sorbitol (Lambros and Vanderberg, 1979). The inhibitors were diluted in DMSO. For the assay, 2 ml of 0.2–0.5% parasitemia culture and different concentrations of RTV and LPV (0.1 μM–10 μM) were added in each well of a 24-well culture plate with growth control and DMSO control. The plates were incubated at 37 °C for 48 h.

The dye dihydroethidium (Sigma-Aldrich) having an $excitation_{max}$/$emission_{max}$ 535/610 nm was used to stain infected red blood cells (iRBCs). The stock solution of dihydroethidium (1 mg/ml) was diluted in phosphate-buffered saline (PBS) (1:2500). 50 μL of the 2% hematocrit blood media mixture (BMM) was pelleted by centrifugation at 1500 rpm for 2 min. The iRBCs were stained by adding 50 μl dihydroethidium working solution (0.63 mM) to iRBCs pellet and incubated in the dark at 37 °C for 25 min. To remove the excess of staining solution, iRBCs were washed with 200 μL PBS, centrifuged at 1500 rpm for 2 min, and finally resuspended in 500 μL PBS (Wirjanata et al., 2015).

Samples were examined using a blue laser (488 nm) BD FACS (Fluorescence-activated cell sorting) AriaIII cytometer system (BD SINGAPORE SORP_Fusion) at the Department of Biosciences and Bioengineering, IIT Bombay. Gating was done according to their FSC-H/SSC-H profile to separate debris from the red blood cell population. Differentiation of cell doublets from single cells was done by gating based on the FSC-A/FSC-W profile. Further, the SSC-A/FITC-A profile was used to analyze stained and unstained singlet RBCs. For data acquisition, 50,000 events were analyzed. The experiments were performed in triplicates, and the graph was plotted using GraphPad Prism with inhibitor concentration versus percent response.

4.5. Crystallization of PMII complexed with ritonavir and lopinavir

Mature PMII (0.1 mM) in the acidic buffer (0.1 M Na acetate pH 4.5) was mixed with a five-fold molar excess of each inhibitor and incubated overnight at 4 °C to form protein-inhibitor complexes. The inhibitors were pre-dissolved in 100 % DMSO and they were added to the protein slowly to avoid sudden precipitation of protein in the presence of DMSO. The mixture was buffer-exchanged in 50 mM phosphate buffer containing 0.15 M NaCl, 0.2% CHAPS pH 7.5, and concentrated using a 10 kDa cut-off ultra-centrifugation device to 8 mg/ml. Crystallization screens of the protein-inhibitor complexes were set up with the help of the Phoenix robotics system (Protein Crystallography Facility, IIT Bombay) using commercial screens from Hampton (Index, PEGIon, PEGRx), Molecular Dimensions (JCSG, JCSG+), and Qiagen (PEG suite). Sitting drops containing 0.3 μl protein solution and 0.3 μl reservoir solution were equilibrated against 50 μl reservoir solution at 293 K. The initial hit of PMII-RTV was observed after a few weeks in the crystallization condition comprising 2.5 M sodium formate, pH 7.0, while crystals of the PMII-LPV complex were observed after several months in a solution containing 1.4 M ammonium sulfate and 0.1 M Bis-Tris pH 5.5.

4.6. Data collection, structure solution, and refinement

The PMII-inhibitor complexed crystals were transferred to cryoprotectant solutions (mother liquor containing 30% ethylene glycol) and then cooled in a nitrogen gas stream at 100 K. The data set for PMII-RTV complex was collected using synchrotron X-ray source at the PX-BL21 beamline (BARC) at Indus-2, Raja Ramanna Centre for Advanced Technology (RRCAT), India, using a MX225 CCD detector. The data set for PMII-LPV complex was collected by the rotation method using a home X-ray radiation source consisting of a Rigaku Micromax 007HF generator equipped with R-Axis IV++ detector at the Protein Crystallography Facility, IIT Bombay. Data sets were indexed and integrated using the program XDS (Kabsch, 2010). Integrated intensities were converted to structure factors with the modules F2MTZ and CAD of CCP4 (Winn et al., 2011).

The coordinates of PMII without the inhibitor (extracted from PDB ID: 5YIC) were used as a search model to solve the structure of the PMII complex with RTV by molecular replacement. Subsequently the coordinates of PMII-RTV complex were used as a search model to solve the structure of the complex of PMII with LPV. After the first cycle of refinement of the model with REFMAC5 (Murshudov et al., 1997) in the CCP4 suite, the sigma-A weighted F_o-F_c electron density maps indicated the presence of inhibitor in the active site pocket of PMII. The ligands were modeled in the F_o-F_c electron density maps. Subsequently, multiple iterative cycles of refinements with REFMAC5 and interactive model building in the electron density map using COOT (Emsley and Cowtan, 2004) were carried out. Local anisotropy was modeled with

translation-libration-screw (TLS) parameters by dividing the protein molecule into distinct TLS groups (Painter and Merritt, 2006). The structures were validated with MolProbity (Davis et al., 2004). The statistics of data collection and refinement are presented in Table 1. All structure-related figures were generated with PyMOL (https://www.pymol.org/).

4.7. Molecular dynamics simulation of a PMX-ritonavir complex

Our attempts to crystallize RTV-bound PMX failed, therefore we performed MD simulation studies for the PMX-RTV complex. The starting structure of PMX used for molecular dynamics (MD) simulations was constructed from the coordinates of the PMX/UCB7362 complex (Lowe et al., 2022) (PDB ID: 8DSR). The inhibitor molecule and the chain B of the structure were removed and the missing residues (Asn346-Asp352) were modeled using SWISS-MODEL (Waterhouse et al., 2018) and added to the experimental structure by using COOT. The binding mode of RTV was identified by a docking based screening method using AutoDockTools-1.5.6 (Morris et al., 2009). MD simulation of the RTV-bound PMX complex was performed with the AMBER99SB-ILDN force field (Lindorff-Larsen et al., 2010) using GROMACS 2019.6 (Van Der Spoel et al., 2005). The parameters for the ligand were generated using *antechamber* program of AmberTools 2021; (Salomon-Ferrer et al. 2013). The topology of the PMX-RTV complex was generated using 'xleap' module of AmberTools. The disulfide bonding pattern of the protein was defined prior to solvation using the TIP3P water model. The cubic solvation box with defined periodic boundary condition has a dimension of 10 Å from the protein to the edge of the box and the system was neutralized by adding a chlorine ion. The topology and coordinate of the PMX-RTV complex generated using 'xleap' module were converted to GROMACS compatible file format using the ParmED (https://parmed.github.io/ParmEd) package. The system was energy minimized using the steepest decent algorithm for 50000 steps with a cutoff of 1000 kJ $mol^{-1}nm^{-1}$; the system was then heated to 310 K using V-rescale (modified Berendsen) thermostat for 100 ps. After NVT equilibration, the system was equilibrated to maintain 1 bar pressure using Berendsen barostat. The covalent bonds with H atoms were constrained using the LINCS algorithm and particle-mesh Ewald (PME) method was used for the long-range electrostatic interactions with a cutoff distance of 1 nm. The heavy atoms were restrained during the equilibration process for the protein-ligand and restraints were removed before the final production run, which was performed for 100 ns with a time step of 2 fs. The trajectories were analyzed using GROMACS 2019.6 and VMD (Humphrey et al., 1996). Figures were created with PyMOL (https://www.pymol.org/).

Table 1
Data collection and refinement statistics of PMII complexed with ritonavir (RTV) and lopinavir (LPV).

	PMII-RTV	PMII-LPV
Data collection statistics[a]		
Space group	*C*2	*I*4
Unit cell parameters *a*, *b*, *c* (Å) *α*, *β*, *γ* (°)	150.29, 70.41, 106.67 90.0, 133.6, 90.0	108.9, 108.9, 70.2 90.0, 90.0, 90.0
Temperature (K)	100	100
Wavelength (Å)	0.9795	1.5419
Resolution (Å)	39.9–1.9 (2.0–1.9)	38.6–3.2 (3.3–3.2)
R_{merge} (%)	4.9 (75.7)	21.0 (231.4)
Completeness (%)	95.9 (96.6)	99.9 (100)
Mean $I/\sigma(I)$	16.16 (1.84)	9.95 (1.04)
Total reflections	177775 (23868)	51868 (4560)
Unique reflections	61329 (8741)	6877 (602)
Redundancy	2.89 (2.73)	7.54 (7.57)
$CC_{1/2}$ (%)	99.9 (65.1)	99.6 (37.5)
Wilson B factor ($Å^2$)	41.24	87.22
No. of molecules in ASU	2	1
Refinement statistics		
Resolution (Å)	39.9–1.9	38.6–3.20
Working set: no. of reflections	58262	6531
R_{factor} (%)	22.26	22.46
Test set: no. of reflections	3067	344
R_{free} (%)	26.13	26.62
Protein atoms	5257	2606
Water molecule	365	0
Inhibitor molecule	Ritonavir (2)	Lopinavir (1)
CHAPS molecule	15	2
Ethylene glycol molecule	2	0
Geometry statistics		
r.m.s.d. bond distance (Å)	0.004	0.004
r.m.s.d. bond angle (°)	1.31	1.44
Isotropic average B-factor ($Å^2$)		
Protein	16.64	50.54
Solvent	53.3	–
Ligand	43.62 (RTV)	98.24 (LPV)
Ramachandran plot		
Most favoured region (%)	96.3	82.6
Allowed regions (%)	3.7	15.3
Outlier (%)	0	2.1
PDB ID	7VE0	7VE2

[a] Values in parentheses correspond to the highest-resolution shell. PMII-RTV: PMII complexed with ritonavir (RTV), PMII-LPV: PMII complexed with lopinavir (LPV).

Author contributions

V.M, I.R., and P.B. conceived the idea and coordinated the study. V. M. prepared the proteins and undertook crystallographic and kinetics experiments under the supervision of P.B. Structure solution and analysis were done by V.M. and I.R. with inputs from P.B. The experimental studies on PMX were performed by A.D. The antiparasitic assays were performed by A.D. with advice from S.P. MD simulations were performed by S. C. The manuscript was jointly written by V.M., I.R., A.D., S. C., A.W. and P.B., with input from the remaining authors.

Declaration of competing interest

The authors declare the following financial interests/personal relationships which may be considered as potential competing interests:

Prasenjit Bhaumik reports financial support was provided by India Ministry of Science & Technology Department of Biotechnology. Alexander Wlodawer reports financial support was provided by Intramural Research Program of the NIH, National Cancer Institute, Center for Cancer Research. Rickey Y. Yada reports financial support was provided by Natural Sciences and Engineering Research Council of Canada. If there are other authors, they declare that they have no known competing financial interests or personal relationships that could have appeared to influence the work reported in this paper.

Data availability

Data will be made available on request.

Acknowledgments

We thank Dr. Ravindra Makde and Dr. Biplab Ghosh at the PX-BL21 beamline (BARC) at Indus-2, RRCAT, Indore, India for their support in diffraction data collection. We acknowledge the Protein Crystallography Facility and the FACS facility at IIT Bombay. We thank Prof. Dominique Soldati-Favre, University of Geneva, Switzerland for providing 49c inhibitor used in our present study. We thank Parijat Das for his help in preparing the graphical abstract. The work was supported in part by the Ramalingaswami Re-entry Fellowship (DBT), a research seed grant from IRCC, IIT Bombay, to Dr. Prasenjit Bhaumik, and in part by the Intramural Research Program of the NIH, National Cancer Institute, Center for Cancer Research. The financial support of the Natural Sciences and

Engineering Research Council of Canada (RYY, RGPIN 04598) is gratefully acknowledged.

Appendix A. Supplementary data

Supplementary data to this article can be found online at https://doi.org/10.1016/j.crstbi.2024.100128.

References

Achan, J., Kakuru, A., Ikilezi, G., Ruel, T., Clark, T.D., Nsanzabana, C., Charlebois, E., Aweeka, F., Dorsey, G., Rosenthal, P.J., Havlir, D., Kamya, M.R., 2012. Antiretroviral agents and Prevention of malaria in HIV-infected Ugandan Children. N. Engl. J. Med. 367, 2110–2118. https://doi.org/10.1056/NEJMoa1200501.

Andrews, K.T., Fairlie, D.P., Madala, P.K., Ray, J., Wyatt, D.M., Hilton, P.M., Melville, L. A., Beattie, L., Gardiner, D.L., Reid, R.C., Stoermer, M.J., Skinner-Adams, T., Berry, C., McCarthy, J.S., 2006. Potencies of human immunodeficiency virus protease inhibitors in vitro against *Plasmodium falciparum* and in vivo against murine malaria. Antimicrob. Agents Chemother. 50, 639–648. https://doi.org/10.1128/AAC.50.2.639-648.2006.

Asojo, O.A., Afonina, E., Gulnik, S.V., Yu, B., Erickson, J.W., Randad, R., Medjahed, D., Silva, A.M., 2002. Structures of Ser205 mutant plasmepsin II from *Plasmodium falciparum* at 1.8 Å in complex with the inhibitors rs367 and rs370. Acta Crystallogr. Sect. D Biol. Crystallogr. 58, 2001–2008. https://doi.org/10.1107/S0907444902014695.

Asojo, O.A., Gulnik, S.V., Afonina, E., Yu, B., Ellman, J.A., Haque, T.S., Silva, A.M., 2003. Novel uncomplexed and complexed structures of plasmepsin II, an aspartic protease from *Plasmodium falciparum*. J. Mol. Biol. 327, 173–181. https://doi.org/10.1016/S0022-2836(03)00036-6.

Banerjee, R., Liu, J., Beatty, W., Pelosof, L., Klemba, M., Goldberg, D.E., 2002. Four plasmepsins are active in the *Plasmodium falciparum* food vacuole, including a protease with an active-site histidine. Proc. Natl. Acad. Sci. U. S. A. 99, 990–995. https://doi.org/10.1073/pnas.022630099.

Bedi, Rajiv K., Patel, C., Mishra, V., Xiao, H., Yada, R.Y., Bhaumik, P., 2016. Understanding the structural basis of substrate recognition by Plasmodium falciparum plasmepsin v to aid in the design of potent inhibitors. Sci. Rep. 6, 1–17. https://doi.org/10.1038/srep31420.

Behnen, J., Köster, H., Neudert, G., Craan, T., Heine, A., Klebe, G., 2012. Experimental and computational active site Mapping as a starting Point to Fragment-based lead discovery. ChemMedChem 7, 248–261. https://doi.org/10.1002/cmdc.201100490.

Bhaumik, P., Gustchina, A., Wlodawer, A., 2012. Structural studies of vacuolar plasmepsins. Biochim. Biophys. Acta, Proteins Proteomics 1824, 207–223. https://doi.org/10.1016/j.bbapap.2011.04.008.

Boddey, J.A., Hodder, A.N., Günther, S., Gilson, P.R., Patsiouras, H., Kapp, E.A., Pearce, J.A., de Koning-Ward, T.F., Simpson, R.J., Crabb, B.S., Cowman, A.F., 2010. An aspartyl protease directs malaria effector proteins to the host cell. Nature 463, 627–631. https://doi.org/10.1038/nature08728.

Boss, C., Corminboeuf, O., Grisostomi, C., Meyer, S., Jones, A.F., Prade, L., Binkert, C., Fischli, W., Weller, T., Bur, D., 2006. Achiral, cheap, and potent inhibitors of plasmepsins I, II, and IV. ChemMedChem 1, 1341–1345. https://doi.org/10.1002/cmdc.200600223.

Cheng, Y., Prusoff, W.H., 1973. Relationship between the inhibition constant (K1) and the concentration of inhibitor which causes 50 per cent inhibition (I50) of an enzymatic reaction. Biochem. Pharmacol. 22, 3099–3108.

Coombs, G.H., Goldberg, D.E., Klemba, M., Berry, C., Kay, J., Mottram, J.C., 2001. Aspartic proteases of *Plasmodium falciparum* and other parasitic protozoa as drug targets. Trends Parasitol. 17, 532–537. https://doi.org/10.1016/S1471-4922(01)02037-2.

Cranmer, S.L., Magowan, C., Liang, J., Coppel, R.L., Cooke, B.M., 1997. An alternative to serum for cultivation of *Plasmodium falciparum* in vitro. Trans. R. Soc. Trop. Med. Hyg. 91, 363–365. https://doi.org/10.1016/S0035-9203(97)90110-3.

Davis, I.W., Murray, L.W., Richardson, J.S., Richardson, D.C., 2004. MOLPROBITY: structure validation and all-atom contact analysis for nucleic acids and their complexes. Nucleic Acids Res. 32, W615–W619. https://doi.org/10.1093/nar/gkh398.

Dondorp, A.M., Nosten, F., Yi, P., Das, D., Phyo, A.P., Tarning, J., Lwin, K.M., Ariey, F., Hanpithakpong, W., Lee, S.J., Ringwald, P., Silamut, K., Imwong, M., Chotivanich, K., Lim, P., Herdman, T., An, S.S., Yeung, S., Singhasivanon, P., Day, N. P.J., Lindegardh, N., Socheat, D., White, N.J., 2009. Artemisinin resistance in *Plasmodium falciparum* malaria. N. Engl. J. Med. 361, 455–467. https://doi.org/10.1056/NEJMoa0808859.

Emsley, P., Cowtan, K., 2004. Coot: model-building tools for molecular graphics. Acta Crystallogr. Sect. D Biol. Crystallogr. 60, 2126–2132. https://doi.org/10.1107/S0907444904019158.

Favuzza, P., de Lera Ruiz, M., Thompson, J.K., Triglia, T., Ngo, A., Steel, R.W.J., Vavrek, M., Christensen, J., Healer, J., Boyce, C., Guo, Z., Hu, M., Khan, T., Murgolo, N., Zhao, L., Penington, J.S., Reaksudsan, K., Jarman, K., Dietrich, M.H., Richardson, L., Guo, K.-Y., Lopaticki, S., Tham, W.-H., Rottmann, M., Papenfuss, T., Robbins, J.A., Boddey, J.A., Sleebs, B.E., Sabroux, H.J., McCauley, J.A., Olsen, D.B., Cowman, A.F., 2020. Dual plasmepsin-targeting antimalarial agents Disrupt multiple stages of the malaria parasite life cycle. Cell Host Microbe 27, 642–658.e12. https://doi.org/10.1016/j.chom.2020.02.005.

Gong, Y., Haque, S., Chowdhury, P., Cory, T.J., Kodidela, S., Yallapu, M.M., Norwood, J. M., Kumar, S., 2019. Pharmacokinetics and pharmacodynamics of cytochrome P450 inhibitors for HIV treatment. Expert Opin. Drug Metab. Toxicol. 15, 417–427. https://doi.org/10.1080/17425255.2019.1604685.

He, Z., Chen, L., You, J., Qin, L., Chen, X., 2010. In vitro interactions between antiretroviral protease inhibitors and artemisinin endoperoxides against *Plasmodium falciparum*. Int. J. Antimicrob. Agents 35, 191–193. https://doi.org/10.1016/j.ijantimicag.2009.09.016.

Hobbs, C.V., Voza, T., Coppi, A., Kirmse, B., Marsh, K., Borkowsky, W., Sinnis, P., 2009. HIV protease inhibitors inhibit the development of Preerythrocytic-stage *Plasmodium* parasites. J. Infect. Dis. 199, 134–141. https://doi.org/10.1086/594369.

Hodder, A.N., Christensen, J., Scally, S., Triglia, T., Ngo, A., Birkinshaw, R.W., Bailey, B., Favuzza, P., Dietrich, M.H., Tham, W.-H., Czabotar, P.E., Lowes, K., Guo, Z., Murgolo, N., Lera Ruiz, M. de, McCauley, J.A., Sleebs, B.E., Olsen, D., Cowman, A.F., 2022. Basis for drug selectivity of plasmepsin IX and X inhibition in *Plasmodium falciparum* and vivax. Structure 30, 947–961.e6. https://doi.org/10.1016/j.str.2022.03.018.

Humphrey, W., Dalke, A., Schulten, K., 1996. VMD: Visual molecular dynamics. J. Mol. Graph. 14, 33–38. https://doi.org/10.1016/0263-7855(96)00018-5.

Istvan, E.S., Goldberg, D.E., 2005. Distal substrate interactions enhance plasmepsin activity. J. Biol. Chem. 280, 6890–6896. https://doi.org/10.1074/jbc.M412086200.

Jaudzems, K., Tars, K., Maurops, G., Ivdra, N., Otikovs, M., Leitans, J., Kanepe-Lapsa, I., Domraceva, I., Mutule, I., Trapencieris, P., Blackman, M.J., Jirgensons, A., 2014. Plasmepsin inhibitory activity and structure-guided optimization of a potent hydroxyethylamine-based antimalarial hit. ACS Med. Chem. Lett. 5, 373–377. https://doi.org/10.1021/ml4004952.

Kabsch, W., 2010. XDS. Acta Crystallogr. D. Biol. Crystallogr. 66, 125–132. https://doi.org/10.1107/S0907444909047337.

Kesari, P., Deshmukh, A., Pahelkar, N., Suryawanshi, A.B., Rathore, I., Mishra, V., Dupuis, J.H., Xiao, H., Gustchina, A., Abendroth, J., Labaied, M., Yada, R.Y., Wlodawer, A., Edwards, T.E., Lorimer, D.D., Bhaumik, P., 2022. Structures of plasmepsin X from *Plasmodium falciparum* reveal a novel inactivation mechanism of the zymogen and molecular basis for binding of inhibitors in mature enzyme. Protein Sci. 31, 882–899. https://doi.org/10.1002/pro.4279.

Kraft, T.E., Armstrong, C., Heitmeier, M.R., Odom, A.R., Hruz, P.W., 2015. The glucose transporter PfHT1 is an antimalarial target of the HIV protease inhibitor lopinavir. Antimicrob. Agents Chemother. 59, 6203–6209. https://doi.org/10.1128/AAC.00899-15.

Lambros, C., Vanderberg, J.P., 1979. Synchronization of *Plasmodium falciparum* erythrocytic stages in culture. J. Parasitol. 65, 418–420.

Lindorff-Larsen, K., Piana, S., Palmo, K., Maragakis, P., Klepeis, J.L., Dror, R.O., Shaw, D. E., 2010. Improved side-chain torsion potentials for the Amber ff99SB protein force field. Proteins Struct. Funct. Bioinforma. 78, 1950–1958. https://doi.org/10.1002/prot.22711.

Lowe, M.A., Cardenas, A., Valentin, J.-P., Zhu, Z., Abendroth, J., Castro, J.L., Class, R., Delaunois, A., Fleurance, R., Gerets, H., Gryshkova, V., King, L., Lorimer, D.D., MacCoss, M., Rowley, J.H., Rosseels, M.-L., Royer, L., Taylor, R.D., Wong, M., Zaccheo, O., Chavan, V.P., Ghule, G.A., Tapkir, B.K., Burrows, J.N., Duffey, M., Rottmann, M., Wittlin, S., Angulo-Barturen, I., Jiménez-Díaz, M.B., Striepen, J., Fairhurst, K.J., Yeo, T., Fidock, D.A., Cowman, A.F., Favuzza, P., Crespo-Fernandez, B., Gamo, F.J., Goldberg, D.E., Soldati-Favre, D., Laleu, B., de Haro, T., 2022. Discovery and Characterization of potent, Efficacious, Orally available antimalarial plasmepsin X inhibitors and Preclinical Safety Assessment of UCB7362. J. Med. Chem. 65, 14121–14143. https://doi.org/10.1021/acs.jmedchem.2c01336.

Mahmoudi, N., Garcia-Domenech, R., Galvez, J., Farhati, K., Franetich, J.-F., Sauerwein, R., Hannoun, L., Derouin, F., Danis, M., Mazier, D., 2008. New active drugs against liver stages of Plasmodium Predicted by molecular topology. Antimicrob. Agents Chemother. 52, 1215–1220. https://doi.org/10.1128/AAC.01043-07.

Matthews, B.W., 1968. Solvent content of protein crystals. J. Mol. Biol. 33, 491–497.

Mishra, L.C., Bhattacharya, A., Sharma, M., Bhasin, V.K., 2010. Short report: HIV protease inhibitors, indinavir or nelfinavir, augment antimalarial action of artemisinin in vitro. Am. J. Trop. Med. Hyg. 82, 148–150. https://doi.org/10.4269/ajtmh.2010.09-0427.

Mishra, V., Rathore, I., Arekar, A., Sthanam, L.K., Xiao, H., Kiso, Y., Sen, S., Patankar, S., Gustchina, A., Hidaka, K., Wlodawer, A., Yada, R.Y., Bhaumik, P., 2018. Deciphering the mechanism of potent peptidomimetic inhibitors targeting plasmepsins – biochemical and structural insights. FEBS J. 285, 3077–3096. https://doi.org/10.1111/febs.14598.

Morris, G.M., Huey, R., Lindstrom, W., Sanner, M.F., Belew, R.K., Goodsell, D.S., Olson, A.J., 2009. AutoDock4 and AutoDockTools4: Automated docking with selective receptor flexibility. J. Comput. Chem. 30, 2785–2791. https://doi.org/10.1002/jcc.21256.

Murshudov, G.N., Vagin, A.A., Dodson, E.J., 1997. Refinement of Macromolecular structures by the Maximum-Likelihood method. Acta Crystallogr. Sect. D Biol. Crystallogr. 53, 240–255. https://doi.org/10.1107/S0907444996012255.

Nasamu, A.S., Glushakova, S., Russo, I., Vaupel, B., Oksman, A., Kim, A.S., Fremont, D. H., Tolia, N., Beck, J.R., Meyers, M.J., Niles, J.C., Zimmerberg, J., Goldberg, D.E., 2017. Plasmepsins IX and X are essential and druggable mediators of malaria parasite egress and invasion. Science 358, 518–522. https://doi.org/10.1126/science.aan1478.

Omara-Opyene, A.L., Moura, P.A., Sulsona, C.R., Bonilla, J.A., Yowell, C.A., Fujioka, H., Fidock, D.A., Dame, J.B., 2004. Genetic Disruption of the *Plasmodium falciparum* digestive vacuole plasmepsins demonstrates their functional redundancy. J. Biol. Chem. 279, 54088–54096. https://doi.org/10.1074/jbc.M409605200.

Onchieku, N.M., Mogire, R., Ndung'u, L., Mwitari, P., Kimani, F., Matoke-Muhia, D., Kiboi, D., Magoma, G., 2018. Deciphering the targets of retroviral protease inhibitors in *Plasmodium berghei*. PLoS One 13, 1–16. https://doi.org/10.1371/journal.pone.0201556.

Painter, J., Merritt, E.A., 2006. Optimal description of a protein structure in terms of multiple groups undergoing TLS motion. Acta Crystallogr. Sect. D Biol. Crystallogr. 62, 439–450. https://doi.org/10.1107/S0907444906005270.

Parikh, S., Gut, J., Istvan, E., Goldberg, D.E., Havlir, D.V., Rosenthal, P.J., 2005. Antimalarial activity of human immunodeficiency virus type 1 protease inhibitors. Antimicrob. Agents Chemother. 49, 2983–2985. https://doi.org/10.1128/AAC.49.7.2983-2985.2005.

Pino, P., Caldelari, R., Mukherjee, B., Vahokoski, J., Klages, N., Maco, B., Collins, C.R., Blackman, M.J., Kursula, I., Heussler, V., Brochet, M., Soldati-Favre, D., 2017. A multistage antimalarial targets the plasmepsins IX and X essential for invasion and egress. Science 358, 522–528. https://doi.org/10.1126/science.aaf8675.

Prade, L., Jones, A.F., Boss, C., Richard-Bildstein, S., Meyer, S., Binkert, C., Bur, D., 2005. X-ray structure of plasmepsin II complexed with a potent achiral inhibitor. J. Biol. Chem. 280, 23837–23843. https://doi.org/10.1074/jbc.M501519200.

Pushpakom, S., Iorio, F., Eyers, P.A., Escott, K.J., Hopper, S., Wells, A., Doig, A., Guilliams, T., Latimer, J., McNamee, C., Norris, A., Sanseau, P., Cavalla, D., Pirmohamed, M., 2019. Drug repurposing: progress, challenges and recommendations. Nat. Rev. Drug Discov. 18, 41–58. https://doi.org/10.1038/nrd.2018.168.

Recacha, R., Leitans, J., Akopjana, I., Aprupe, L., Trapencieris, P., Jaudzems, K., Jirgensons, A., Tars, K., 2015. Structures of plasmepsin II from *Plasmodium falciparum* in complex with two hydroxyethylamine-based inhibitors. Acta Crystallogr. Sect. Struct. Biol. Commun. 71, 1531–1539. https://doi.org/10.1107/S2053230X15022049.

Rosenthal, P.J., 2003. Antimalarial drug discovery: old and new approaches. J. Exp. Biol. 206, 3735–3744. https://doi.org/10.1242/jeb.00589.

Salomon-Ferrer, R., Case, D.A., Walker, R.C., 2013. An overview of the Amber biomolecular simulation package. WIREs Comput. Mol. Sci. 3, 198–210. https://doi.org/10.1002/wcms.1121.

Silva, A.M., Lee, A.Y., Erickson, J.W., Goldberg, D.E., 1996. Structural analysis of plasmepsin II - a comparison with human aspartic proteases. 7th Int. Conf. Aspartic Proteinases 363–373.

Skinner-Adams, Tina S., McCarthy, J.S., Gardiner, D.L., Hilton, P.M., Andrews, K.T., 2004. Antiretrovirals as antimalarial agents. J. Infect. Dis. 190, 1998–2000. https://doi.org/10.1086/425584.

Van Der Spoel, D., Lindahl, E., Hess, B., Groenhof, G., Mark, A.E., Berendsen, H.J.C., 2005. GROMACS: Fast, flexible, and free. J. Comput. Chem. 26, 1701–1718. https://doi.org/10.1002/jcc.20291.

Waterhouse, A., Bertoni, M., Bienert, S., Studer, G., Tauriello, G., Gumienny, R., Heer, F. T., de Beer, T.A.P., Rempfer, C., Bordoli, L., Lepore, R., Schwede, T., 2018. SWISS-MODEL: homology modelling of protein structures and complexes. Nucleic Acids Res. 46, W296–W303. https://doi.org/10.1093/nar/gky427.

White, N.J., Pukrittayakamee, S., Hien, T.T., Faiz, M.A., Mokuolu, O.A., Dondorp, A.M., 2014. Malaria. Lancet 383, 723–735. https://doi.org/10.1016/S0140-6736(13)60024-0.

Winn, M.D., Ballard, C.C., Cowtan, K.D., Dodson, E.J., Emsley, P., Evans, P.R., Keegan, R. M., Krissinel, E.B., Leslie, A.G.W., McCoy, A., McNicholas, S.J., Murshudov, G.N., Pannu, N.S., Potterton, E.A., Powell, H.R., Read, R.J., Vagin, A., Wilson, K.S., 2011. Overview of the CCP 4 suite and current developments. Acta Crystallogr. Sect. D Biol. Crystallogr. 67, 235–242. https://doi.org/10.1107/S0907444910045749.

Wirjanata, G., Handayuni, I., Prayoga, P., Apriyanti, D., Chalfein, F., Sebayang, B.F., Kho, S., Noviyanti, R., Kenangalem, E., Campo, B., Poespoprodjo, J.R., Price, R.N., Marfurt, J., 2015. Quantification of Plasmodium ex vivo drug susceptibility by flow cytometry. Malar. J. 14, 417. https://doi.org/10.1186/s12936-015-0940-8.

World Health Organization, 2022. World Malaria Report 2022. World Heal, Organ.

Zolg, J.W., MacLeod, A.J., Dickson, I.H., Scaife, J.G., 1982. *Plasmodium falciparum*: modifications of the in vitro culture conditions improving parasitic yields. J. Parasitol. 68, 1072–1080.